Supporting Information for

Electrochemical switching of first-generation donor-acceptor Stenhouse adducts (DASAs): An alternative stimulus for triene cyclisation

Nicholas D. Shepherd,[a] Harrison S. Moore,[a] Jonathon E. Beves,[b] Deanna M. D'Alessandro[a]

[a] School of Chemistry, The University of Sydney, Sydney, NSW 2006, Australia.

[b] School of Chemistry, The University of New South Wales, Sydney, NSW 2052, Australia.

* deanna.dalessandro@sydney.edu.au

Contents

S1. Experimental

General Characterisation

Solution-state ^{1}H NMR spectra were recorded on a Bruker AVANCEIII 300 MHz spectrometer at 300 K. Chemical shifts (δ) were calibrated against solvent residual signals.[1] Positive and negative ion ESI-MS spectra were obtained using a Bruker amaZon SL mass spectrometer. HPLC grade MeOH was used for serial 10× dilutions. ATR-FTIR spectra were recorded on PerkinElmer Spectrum Two IR spectrometer with UATR attachment. Spectra were recorded with 32 scans at 2 cm^{-1} resolution. Solution UV-vis measurements were carried out using a Cary5000 spectrophotometer. Spectra were collected following irradiation with white LED lights arranged on a breadboard circuit at 20 minute intervals within the range of 10000-30000 cm^{-1}. DASA solutions were prepared through dissolution of the respective compound (*ca.* 2 mg) in MeCN (25 mL) which was diluted by a factor of 100 to yield solutions with concentrations of *ca.* 2.5-2.7 × 10^{-6} M.

DC CV and SQW measurements were conducted with a Bioanalytical Systems Epsilon Electrochemical Analyser potentiostat. Working, auxillary and reference electrodes in the cell were glassy carbon, Pt wire and Ag wire, respectively. 0.1 M $TBAPF_6$ in MeCN acted as the electrolyte which was also used as a blank for detecting impurities that could be present in the cell. All electrolyte solutions were degassed with Ar for a minimum of ten minutes. DASA compounds (*ca.* 1-2 mg) were dissolved in the electrolyte (10 mL) following blank measurements. Experiments involved measuring the current as a function of potential. Scan rates applied are indicated for individual CV data. The ferrocene/ferrocenium (Fc/Fc^+) couple was used as an internal reference for all experimental potentials.

SEC measurements were conducted on the same spectrophotometer previously noted. The solution was analysed in a custom-made quartz optically transparent thin-layer electrochemical (OTTLE) cell with a 0.685 mm pathlength. This OTTLE cell was fused to a quartz cylinder. Working, auxillary and reference electrodes were Pt gauze, Pt wire and Ag wire, respectively. The auxillary and reference electrodes were immersed in sintered frits containing electrolytic solution (0.1 M $TBAPF_6$ in MeCN). The OTTLE cell was covered with a Teflon cap. Baseline correction was conducted using blank electrolytic solution. Samples were prepared through dissolution of 1-2 mg of DASA compounds in electrolytic solution. DASA solutions were further diluted to approximately 2.5-2.7 × 10^{-6} M. Batch collections were performed in continuous mode from 10000-26000 cm^{-1} where scan rates were 7273 and 13636 cm^{-1} min^{-1} in NIR and visible regions, respectively. Potentials were controlled with an eDAQ e-corder 410 potentiostat.

Materials & Syntheses

All chemicals were mostly used as provided by commercial suppliers. MeCN used for electrochemical analyses was dried overnight in CaH_2 and distilled under N_2. $TBAPF_6$ was recrystallised three times in EtOH.

All precursor (**P1** and **P2**) and DASA (**1**-**6**) compounds were prepared in accordance with literature precedent.[2,3] Compound structures were confirmed through ^{1}H NMR and ESI-MS spectroscopies.

S2. ^{1}H Nuclear Magnetic Resonance (NMR) Spectroscopy

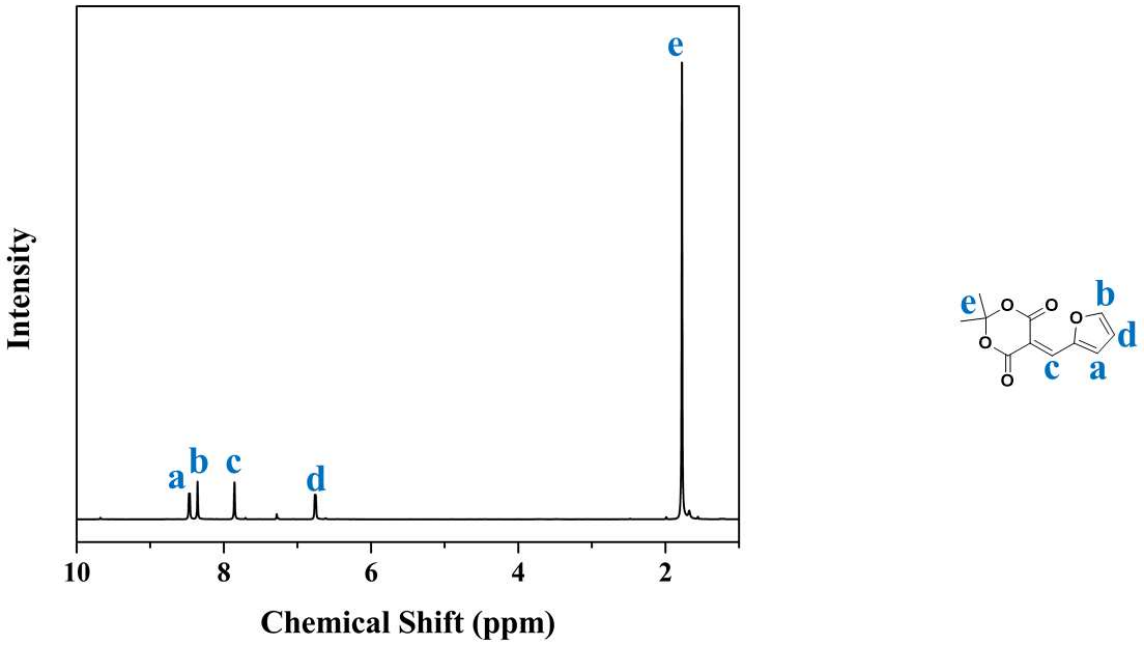

Fig. S1. 300 MHz ^{1}H NMR spectrum of **P1** in $CDCl_3$.

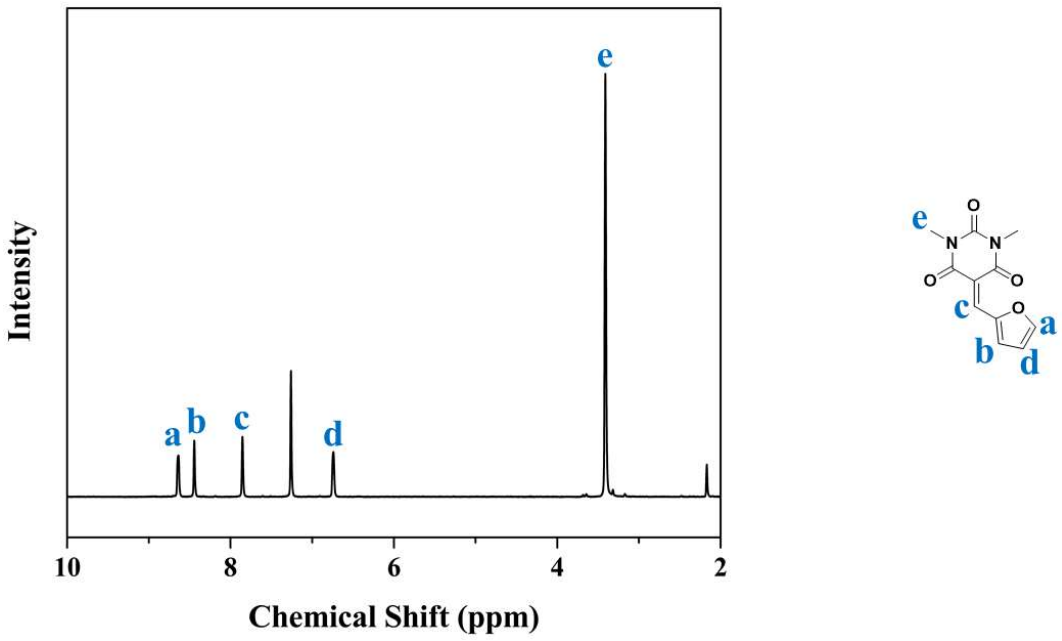

Fig. S2. 300 MHz ^{1}H NMR spectrum of **P2** in $CDCl_3$.

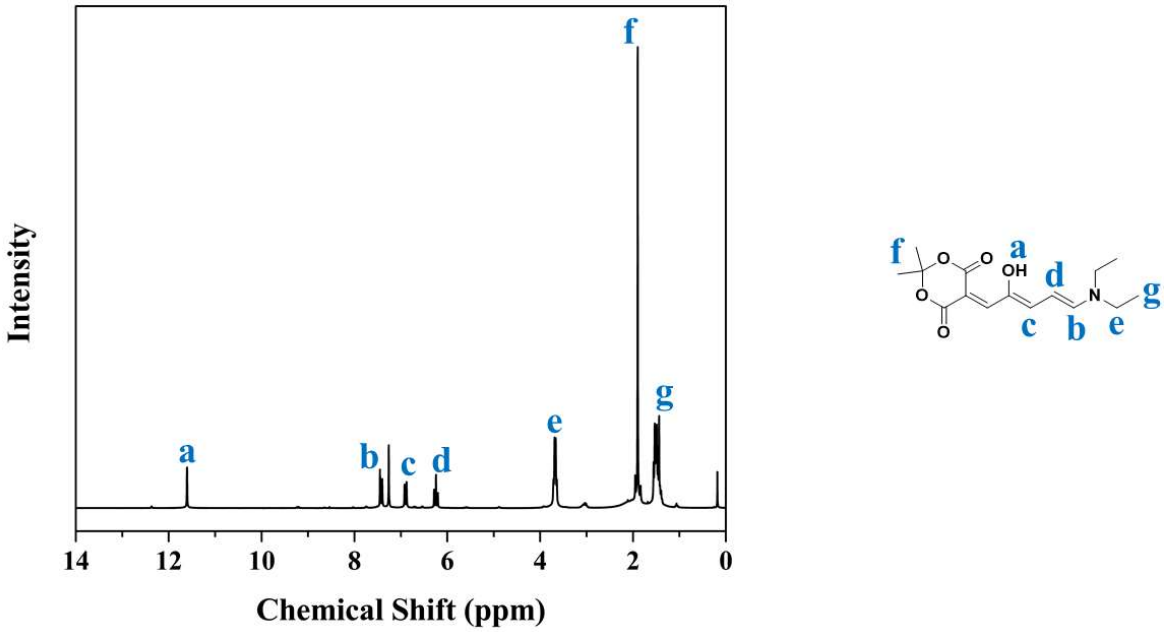

Fig. S3. 300 MHz ^{1}H NMR spectrum of **1** in $CDCl_3$.

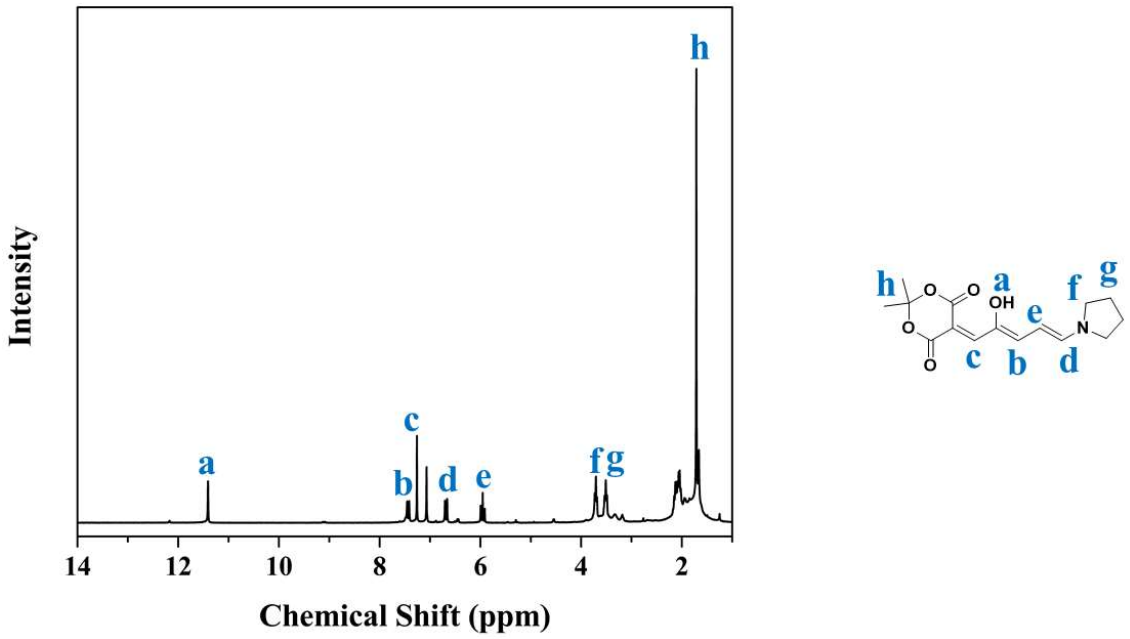

Fig. S4. 300 MHz ^{1}H NMR spectrum of **2** in $CDCl_3$.

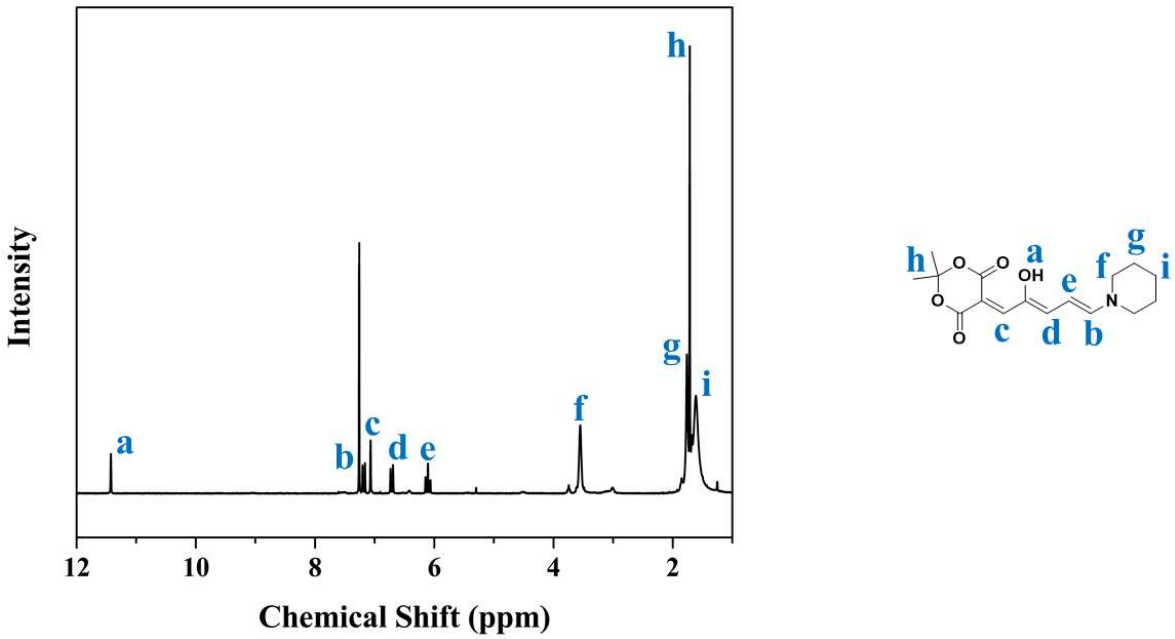

Fig. S5. 300 MHz ^{1}H NMR spectrum of **3** in $CDCl_3$.

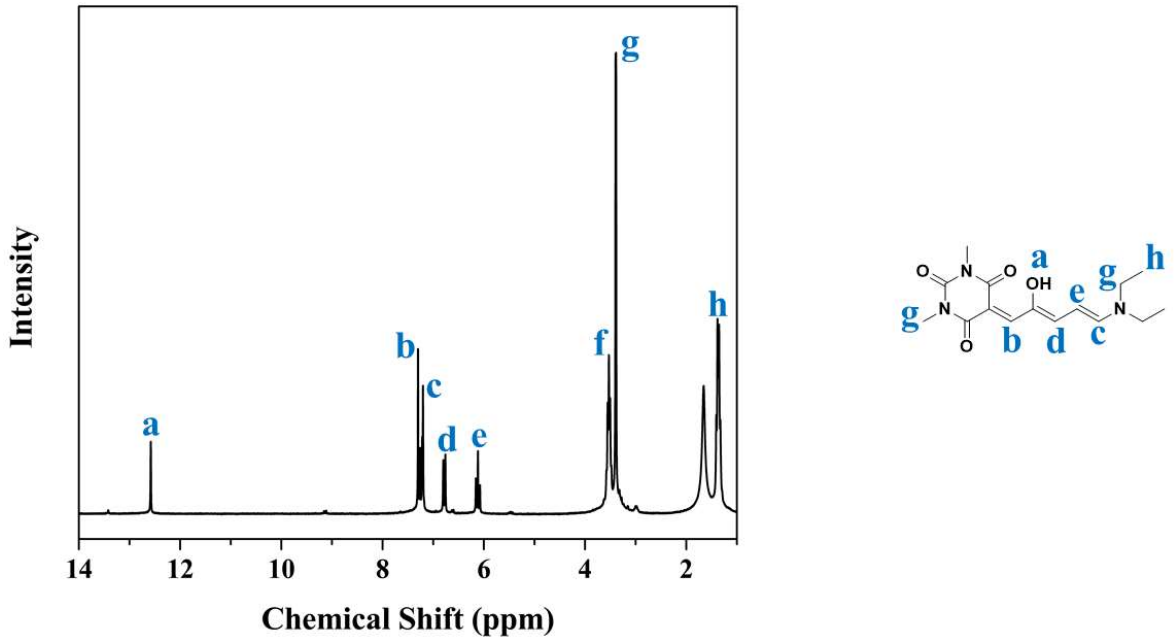

Fig. S6. 300 MHz ^{1}H NMR spectrum of **4** in $CDCl_3$.

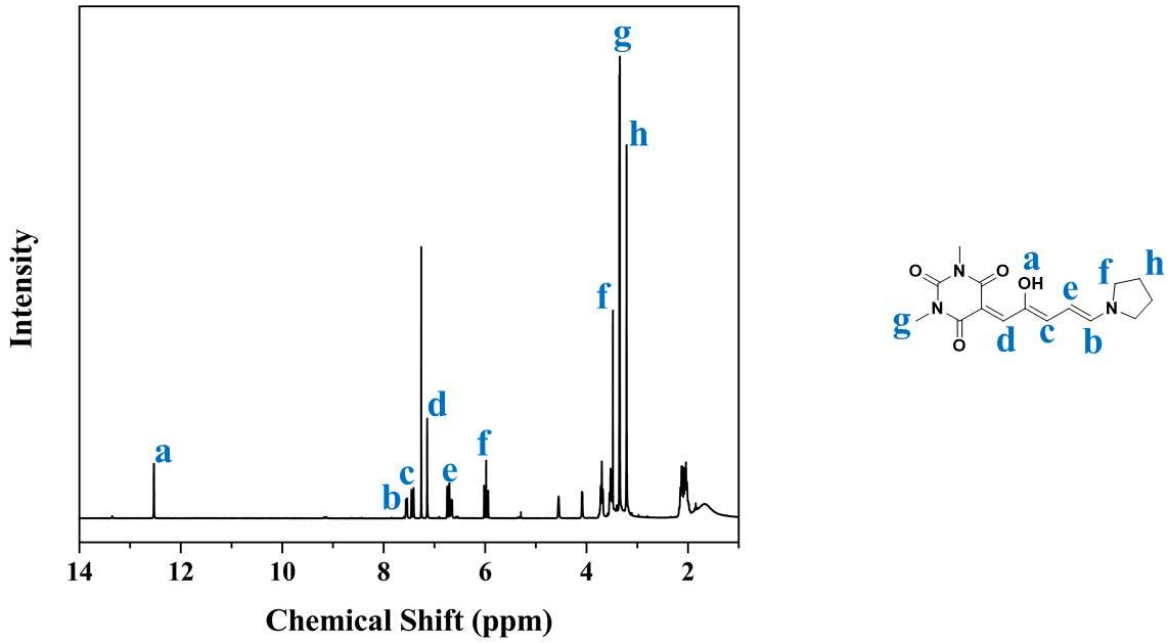

Fig. S7. 300 MHz ^{1}H NMR spectrum of **5** in $CDCl_3$.

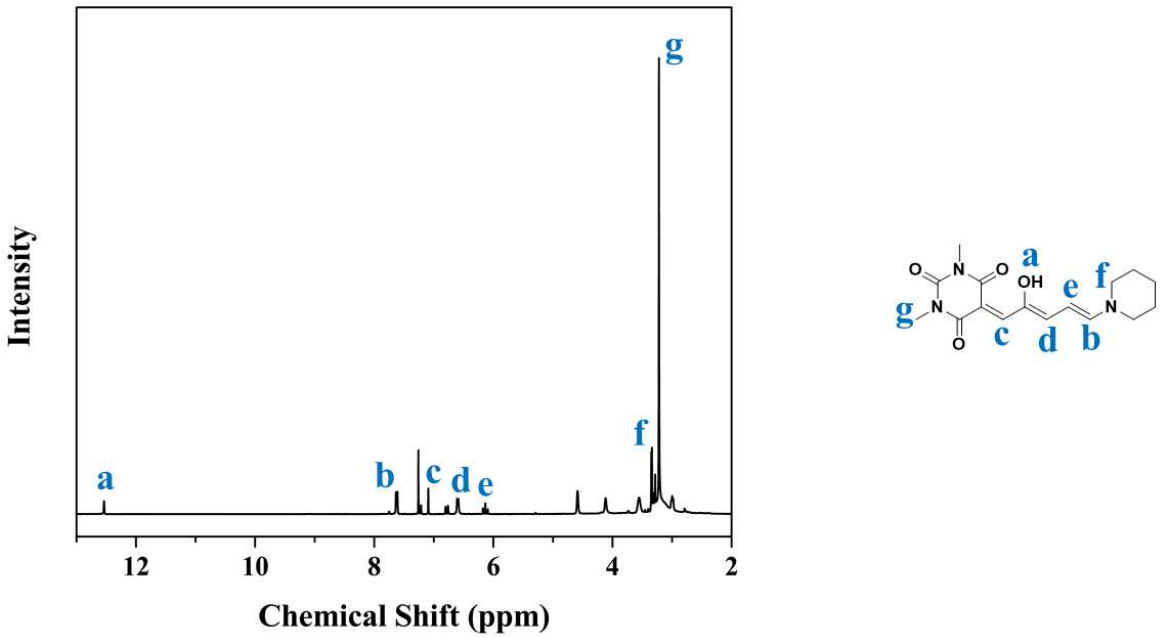

Fig. S8. 300 MHz ^{1}H NMR spectrum of **6** in $CDCl_3$.

S3. Electrospray Ionisation Mass Spectrometry (ESI-MS)

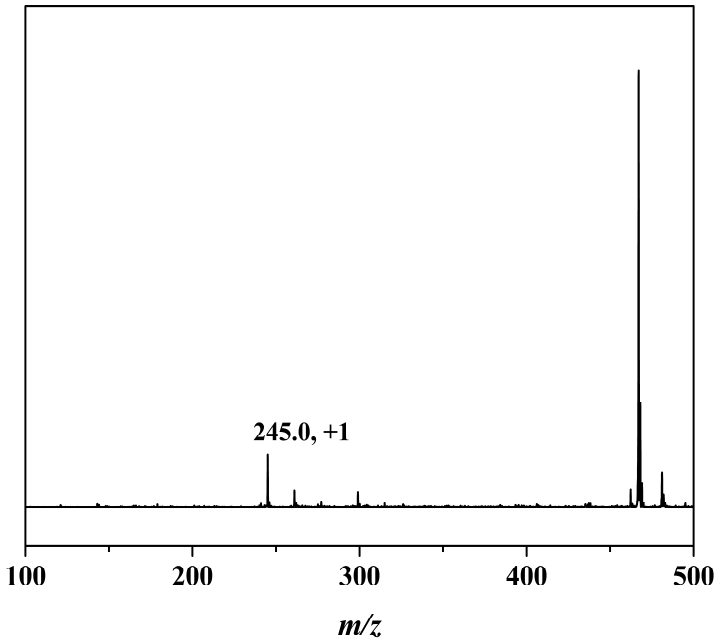

Fig. S9. Positive ion ESI-MS for **P1** in MeOH.

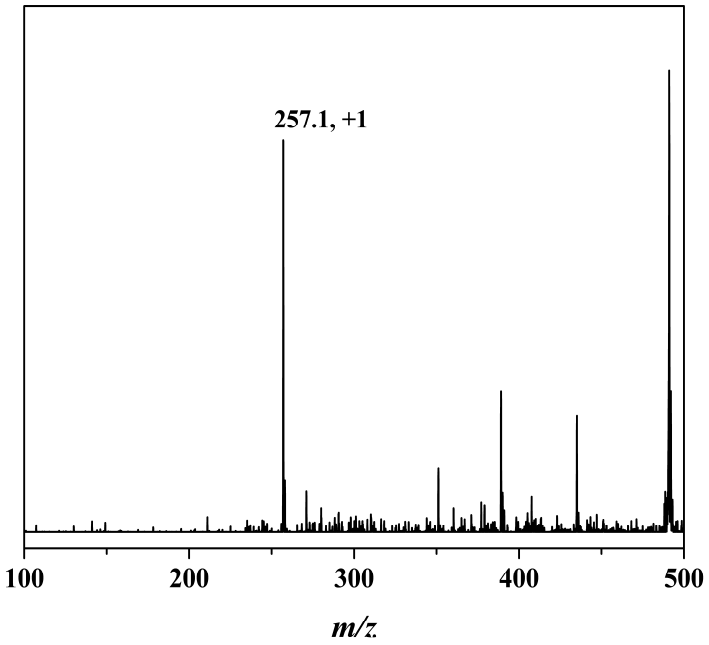

Fig. S10. Positive ion ESI-MS for **P2** in MeOH.

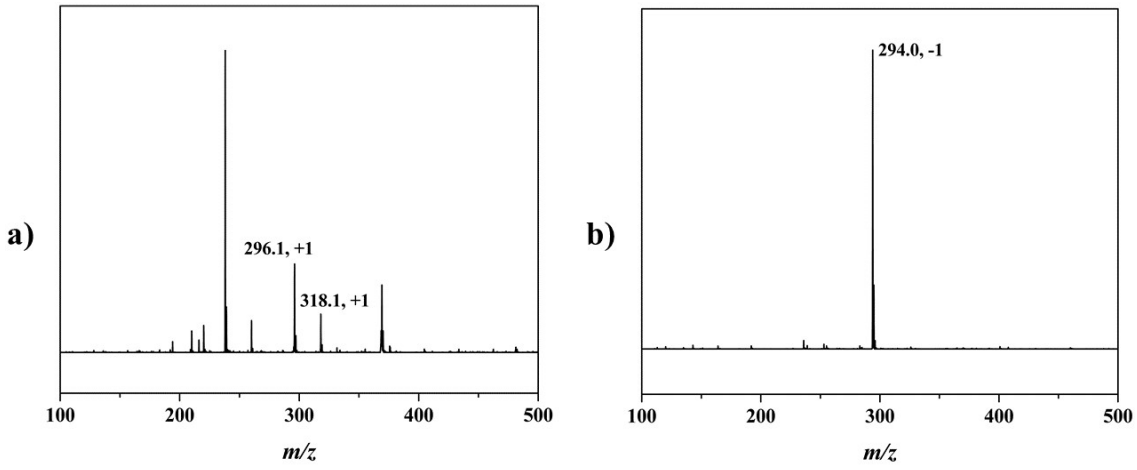

Fig. S11. Positive and negative ion ESI-MS for **1** in MeOH.

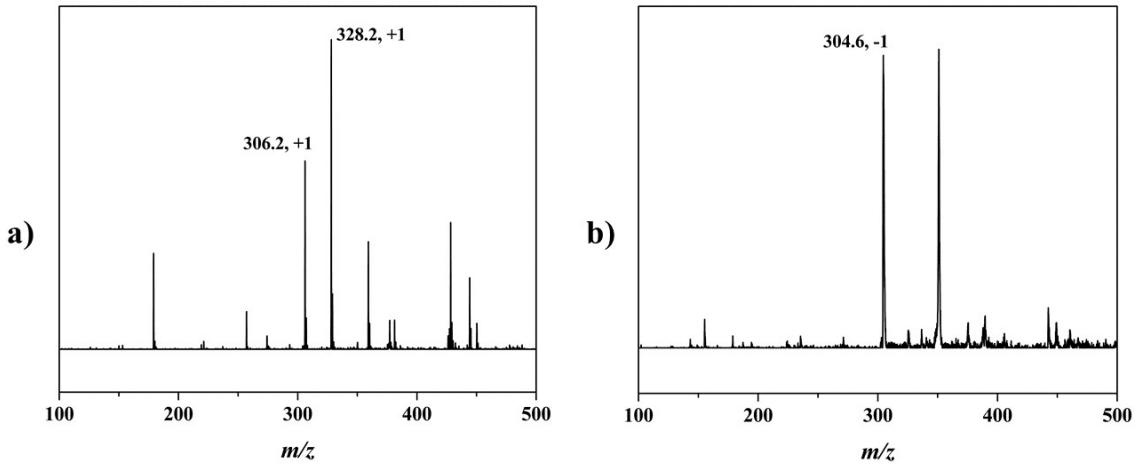

Fig. S12. Positive and negative ion ESI-MS for **2** in MeOH.

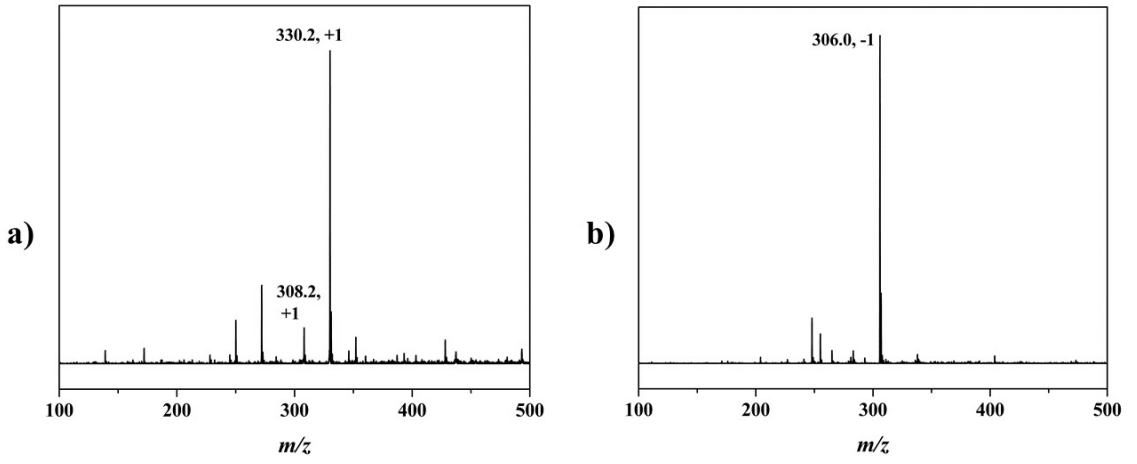

Fig. S13. Positive and negative ion ESI-MS for **3** in MeOH.

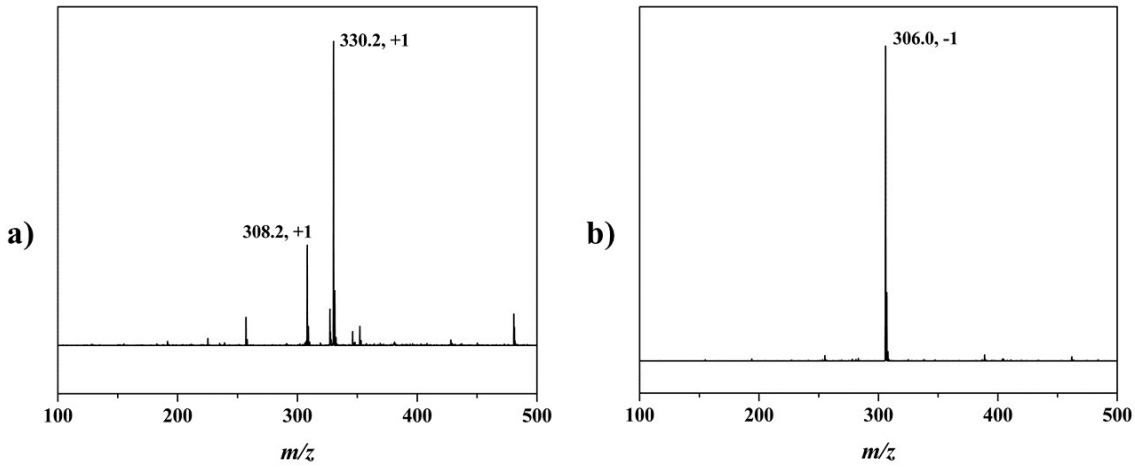

Fig. S14. Positive and negative ion ESI-MS for **4** in MeOH.

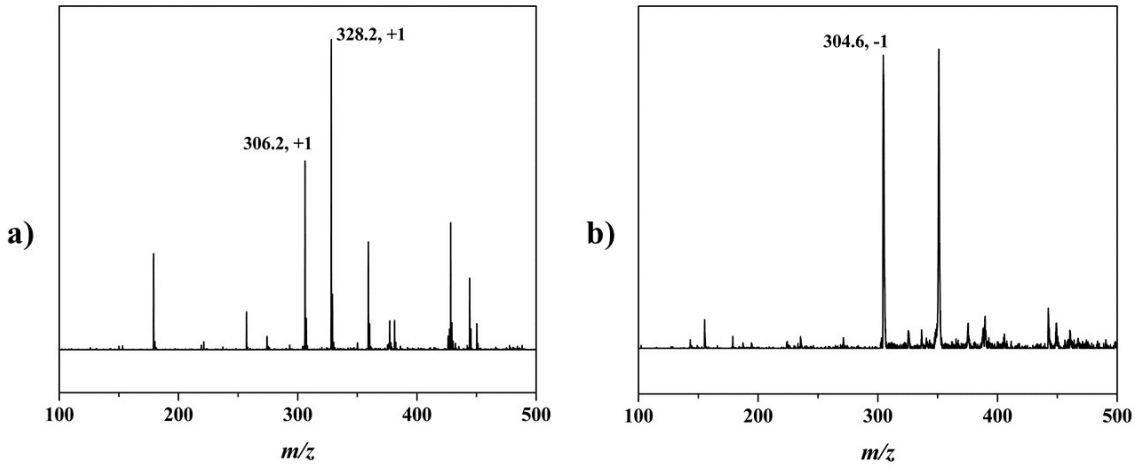

Fig. S15. Positive and negative ion ESI-MS for **5** in MeOH.

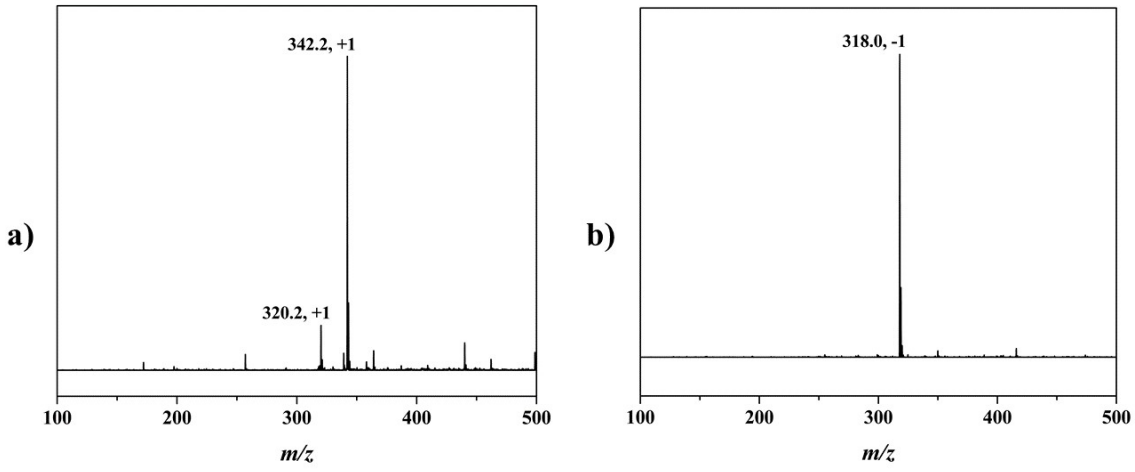

Fig. S16. Positive and negative ion ESI-MS for **6** in MeOH.

S4. Attenuated Reflectance-Fourier Transform Infrared (ATR-FTIR) Spectroscopy

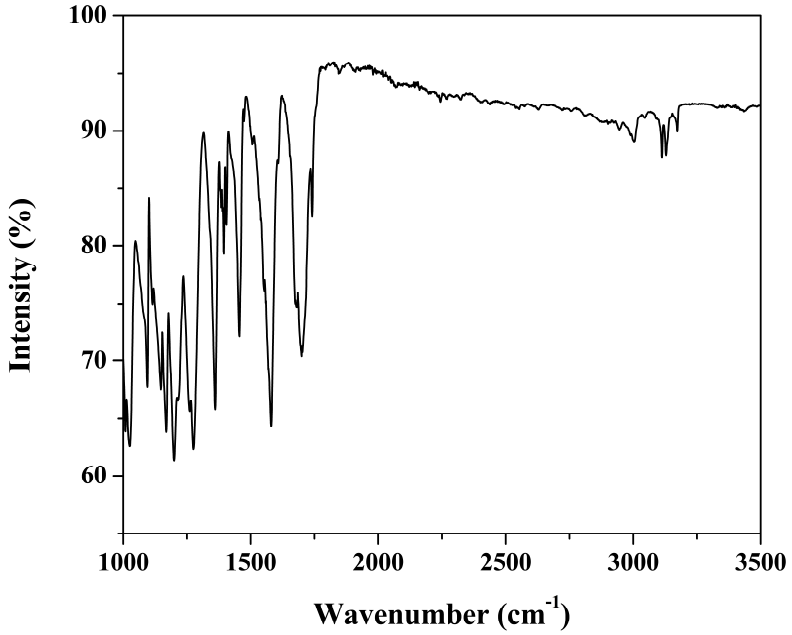

Fig. S17. ATR-FTIR spectrum for **P1** from 1000-3500 cm^{-1}.

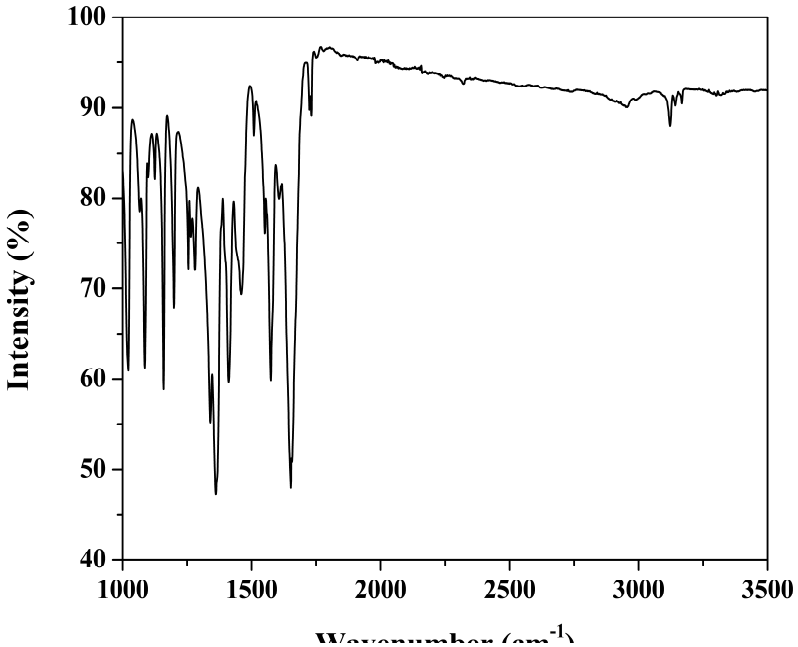

Fig. S18. ATR-FTIR spectrum for **P2** from 1000-3500 cm^{-1}.

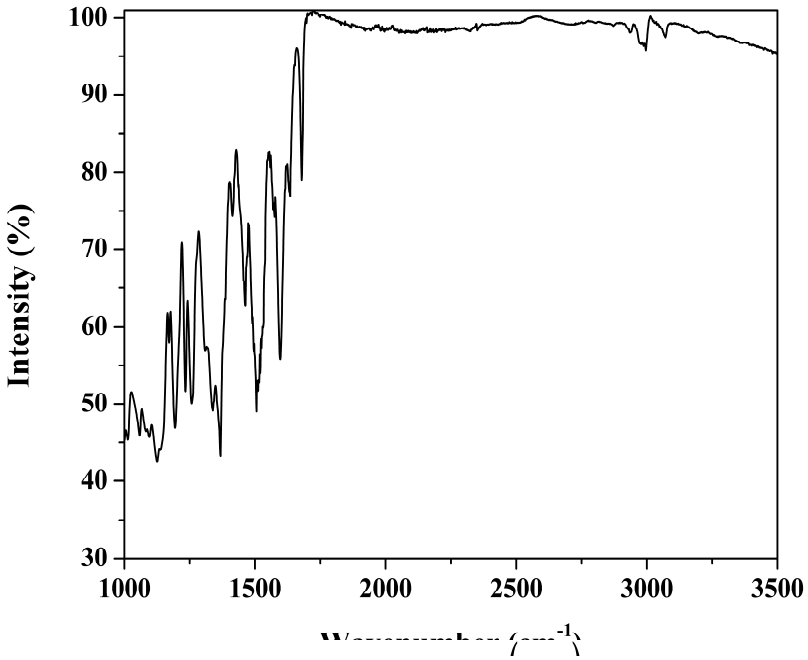

Fig. S19. ATR-FTIR spectrum for **1** from 1000-3500 cm^{-1}.

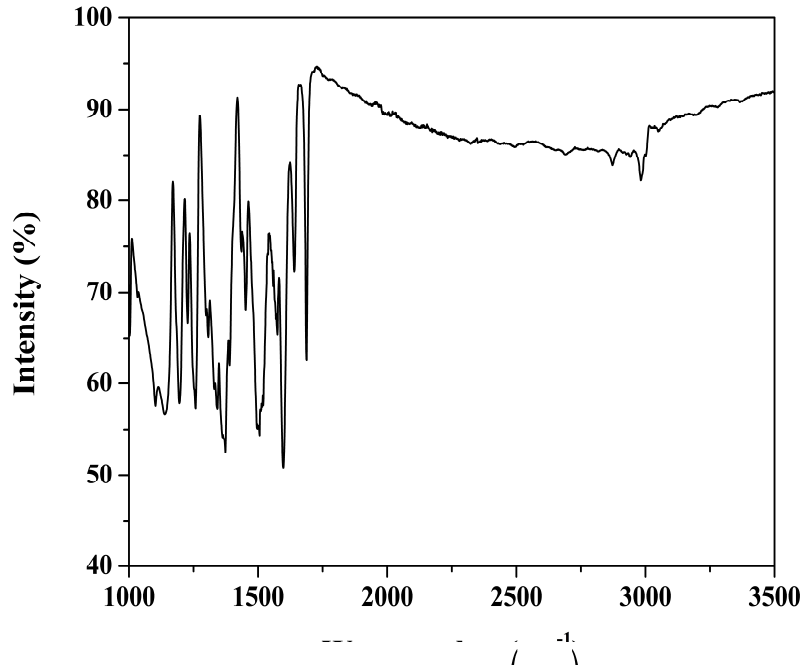

Fig. S20. ATR-FTIR spectrum for **2** from 1000-3500 cm^{-1}.

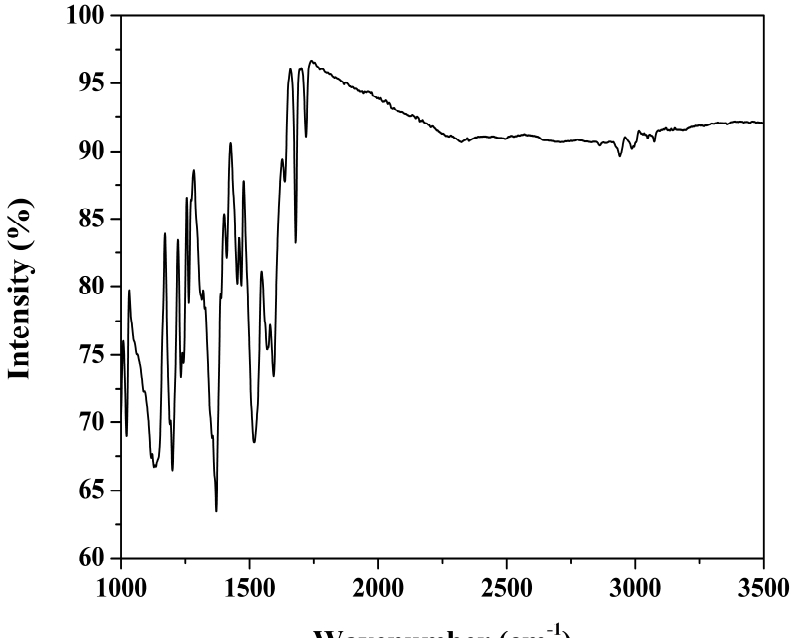

Fig. S21. ATR-FTIR spectrum for **3** from 1000-3500 cm^{-1}.

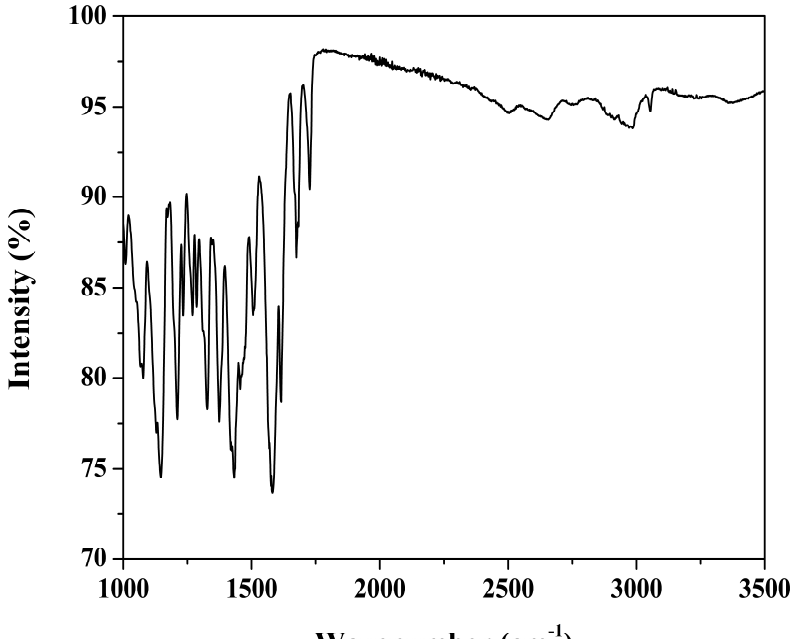

Fig. S22. ATR-FTIR spectrum for **4** from 1000-3500 cm^{-1}.

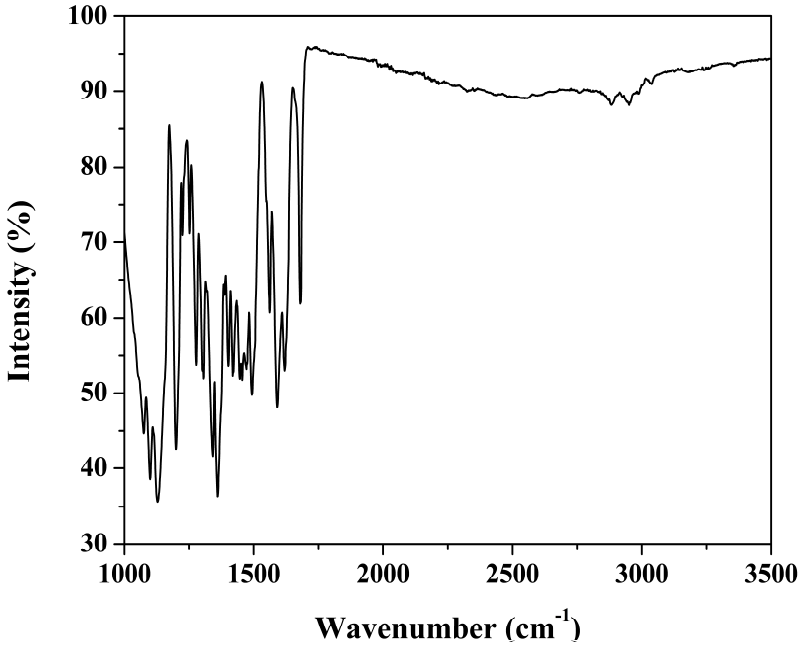

Fig. S23. ATR-FTIR spectrum for **5** from 1000-3500 cm^{-1}.

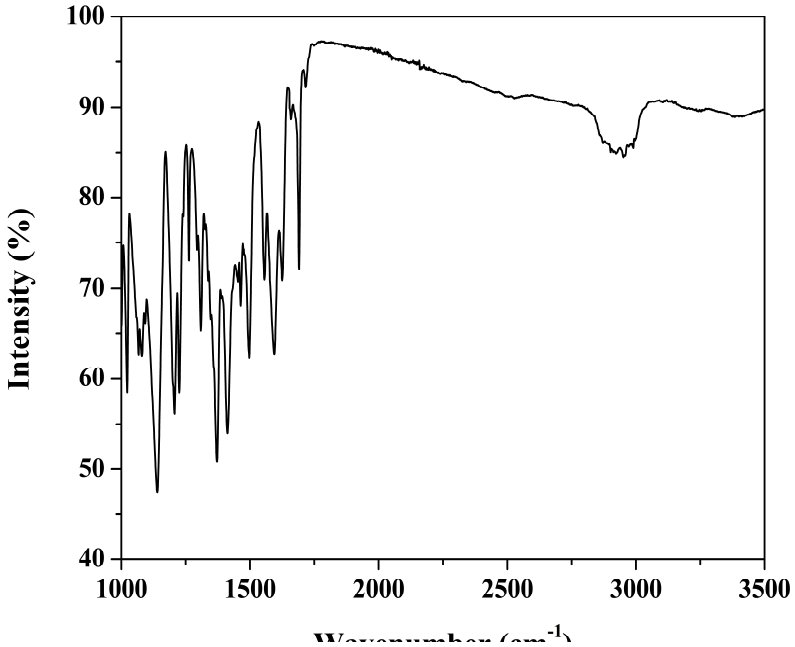

Fig. S24. ATR-FTIR spectrum for **6** from 1000-3500 cm^{-1}.

ATR-FTIR spectra for **1**-**6** (Fig. S19-S24) provided vibrational evidence of successful synthesis. In particular, the appearance of bands at *ca.* 3000 cm^{-1} are consistent with the OH stretch of the alcohol functional group that is unique to the DASAs (compared to their precursors).[4] Additionally, signals detected at *ca.* 1670 cm^{-1} were assigned to the conjugated C=C stretching in the triene chain.[4] Finally, the lack of a peak consistent with the C=H stretches of the activated furan precursor's furan ring (expected within *ca.* 3100-3150 cm^{-1}) was also in keeping with successful DASA synthesis.[4]

S5. Ultraviolet-Visible (UV-Vis) Spectroscopy

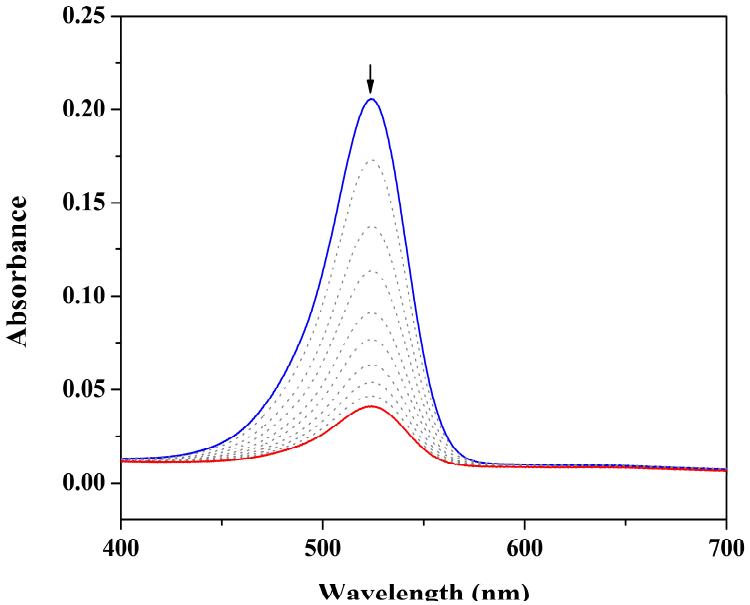

Fig. S25. UV-vis spectra from 400-700 nm for **1** in MeCN. Spectra were collected following white light irradiation (at 20 minute intervals) for up to 180 minutes. The thermodynamic and final irradiation interval spectra are blue and red, respectively.

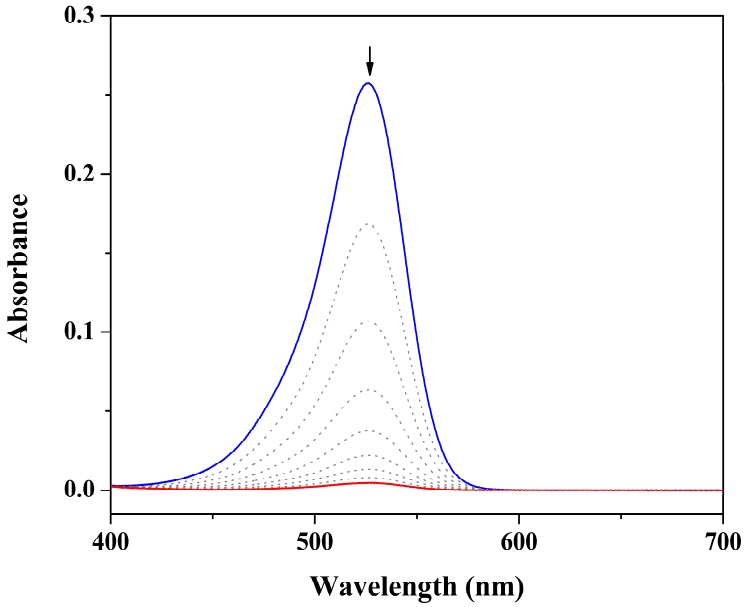

Fig. S26. UV-vis spectra from 400-700 nm for **2** in MeCN. Spectra were collected following white light irradiation (at 20 minute intervals) for up to 160 minutes. The thermodynamic and final irradiation interval spectra are blue and red, respectively.

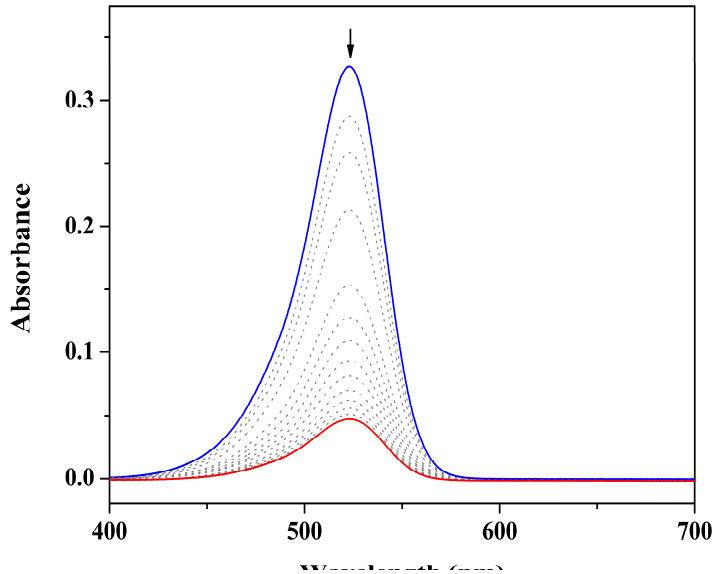

Fig. S27. UV-vis spectra from 400-700 nm for **3** in MeCN. Spectra were collected following white light irradiation (at 20 minute intervals) for up to 260 minutes. The thermodynamic and final irradiation interval spectra are blue and red, respectively.

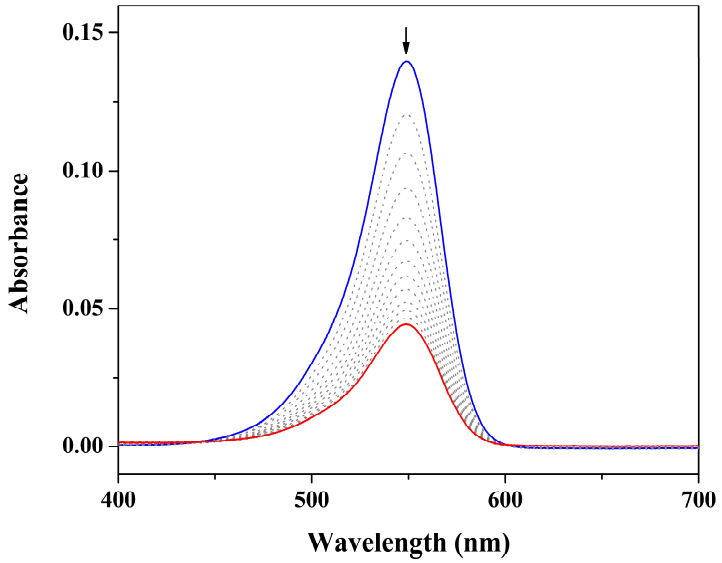

Fig. S28. UV-vis spectra from 400-700 nm for **4** in MeCN. Spectra were collected following white light irradiation (at 20 minute intervals) for up to 240 minutes. The thermodynamic and final irradiation interval spectra are blue and red, respectively.

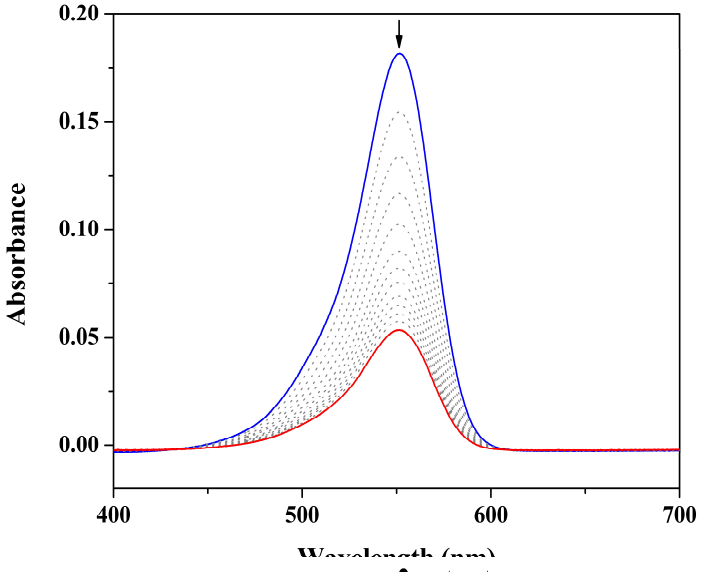

Fig. S29. UV-vis spectra from 400-700 nm for **5** in MeCN. Spectra were collected following white light irradiation (at 20 minute intervals) for up to 240 minutes. The thermodynamic and final irradiation interval spectra are blue and red, respectively.

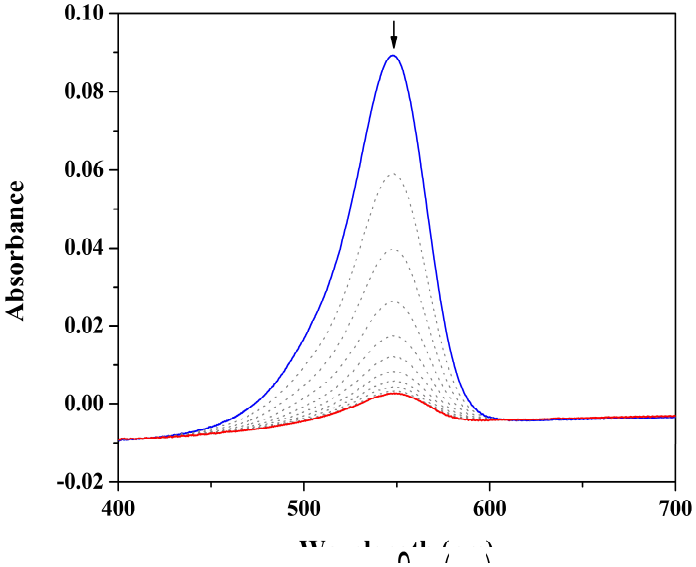

Fig. S30. UV-vis spectra from 400-700 nm for **6** in MeCN. Spectra were collected following white light irradiation (at 10 minute intervals) for up to 100 minutes. The thermodynamic and final irradiation interval spectra are blue and red, respectively.

DASA photo-switching experiments were conducted following dissolution in MeCN. UV-vis spectra for **1**-**6** (Fig. S25-S30) indicated the presence of a band in the visible region that was consistent with the S_0-S_1 transition associated with the triene isomer. Irradiation with white light resulted in this band decreasing in intensity, indicating that the linear thermodynamic configuration was converting to the respective cyclopentenone metastable state. Additionally, a quantitative yield of the metastable state could not be achieved for **1**-**6**.

S6. Voltammetry

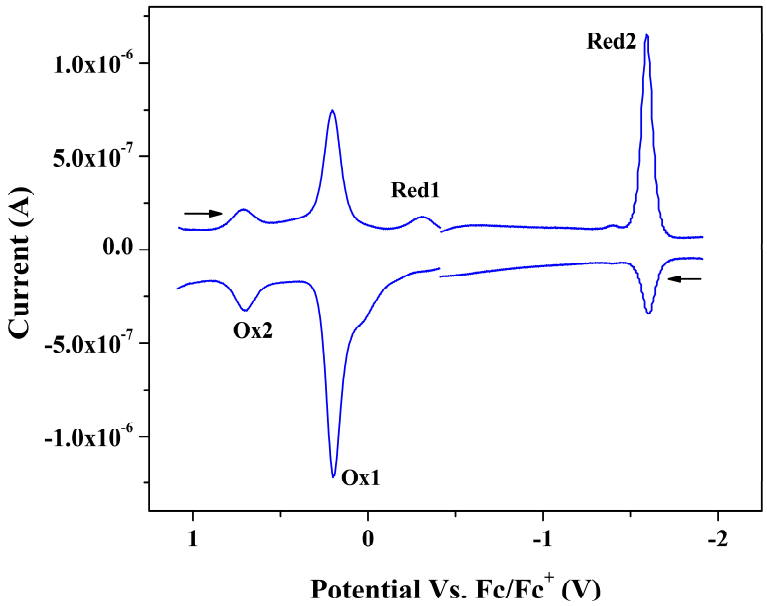

Fig. S31. SQW voltammetry for **1**.

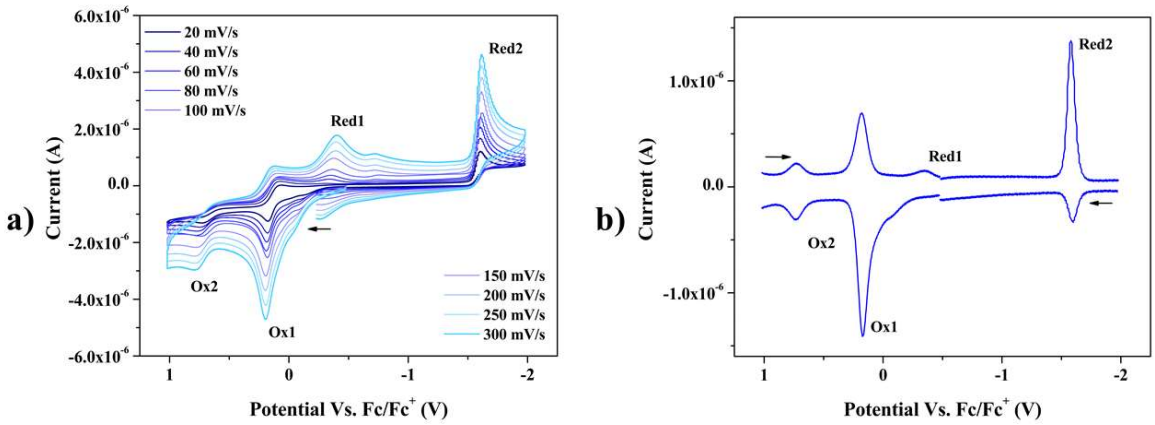

Fig. S32. CV recorded over 20-300 mV/s (a) and SQW voltammetry (b) for **2**.

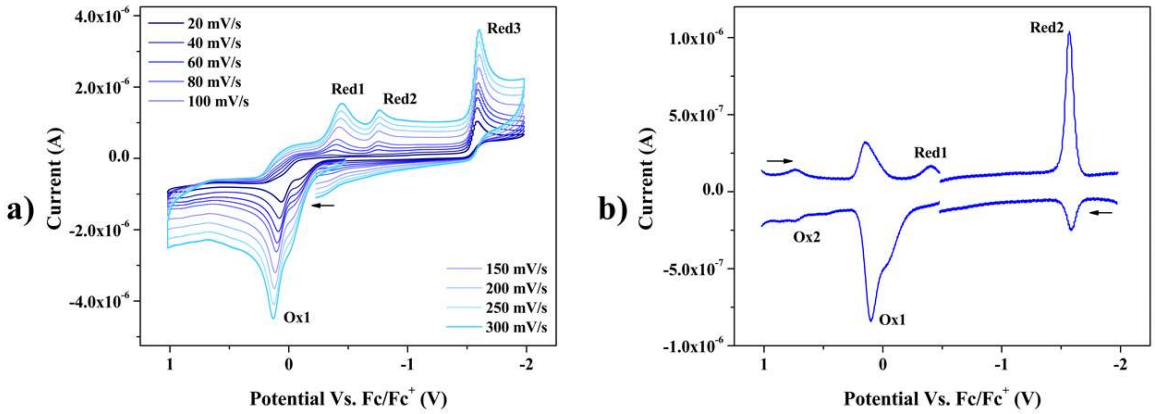

Fig. S33. CV recorded over 20-300 mV/s (a) and SQW voltammetry (b) for **3**.

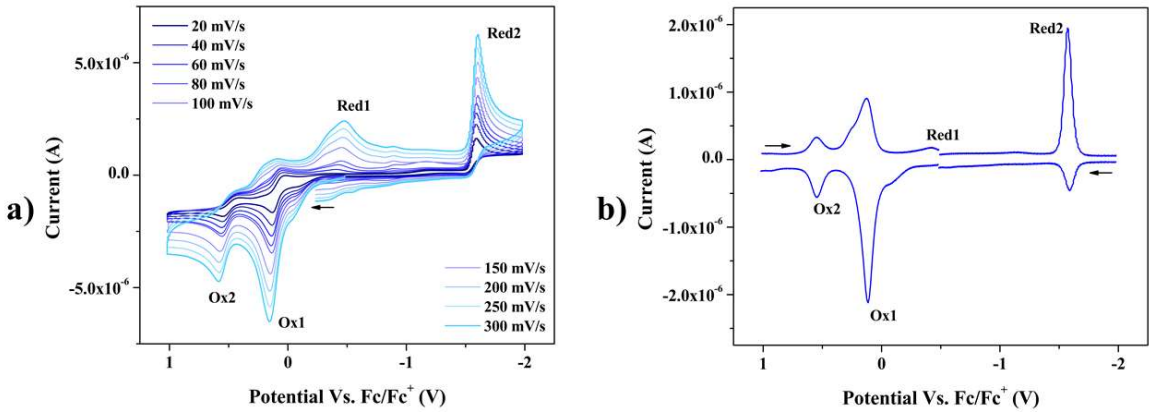

Fig. S34. CV recorded over 20-300 mV/s (a) and SQW voltammetry (b) for **4**.

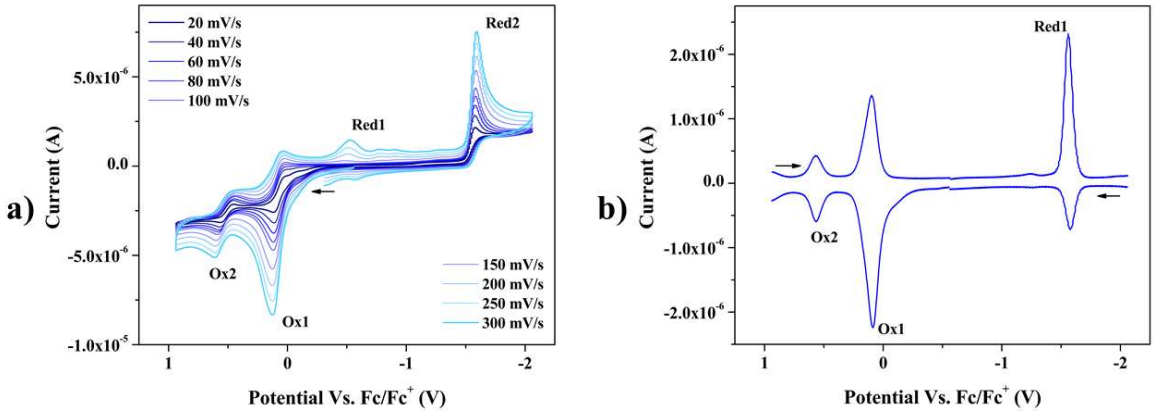

Fig. S35. CV recorded over 20-300 mV/s (a) and SQW voltammetry (b) for **5**.

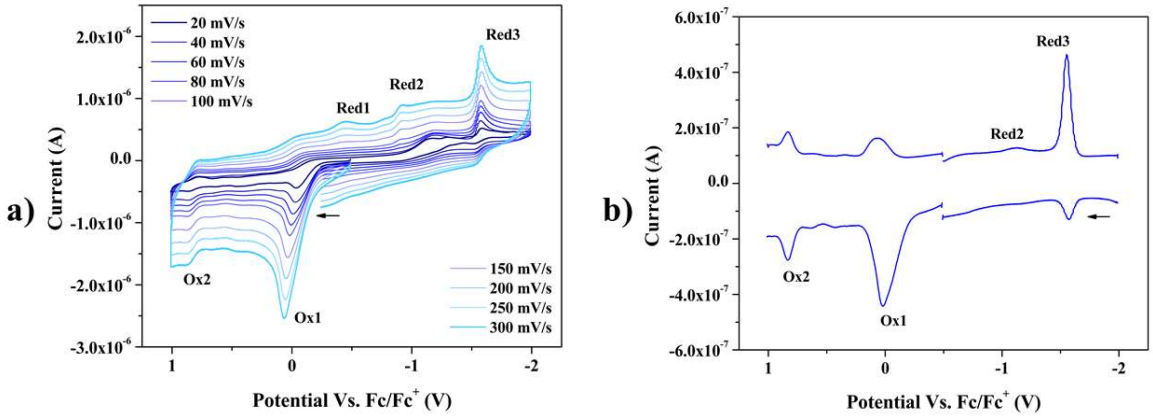

Fig. S36. CV recorded over 20-300 mV/s (a) and SQW voltammetry (b) for **6**.

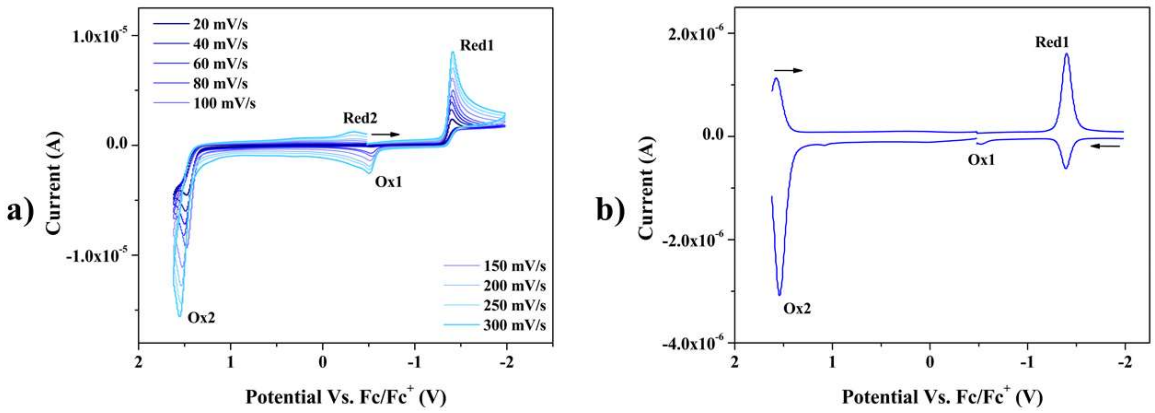

Fig. S37. CV recorded over 20-300 mV/s (a) and SQW voltammetry (b) for **P1**.

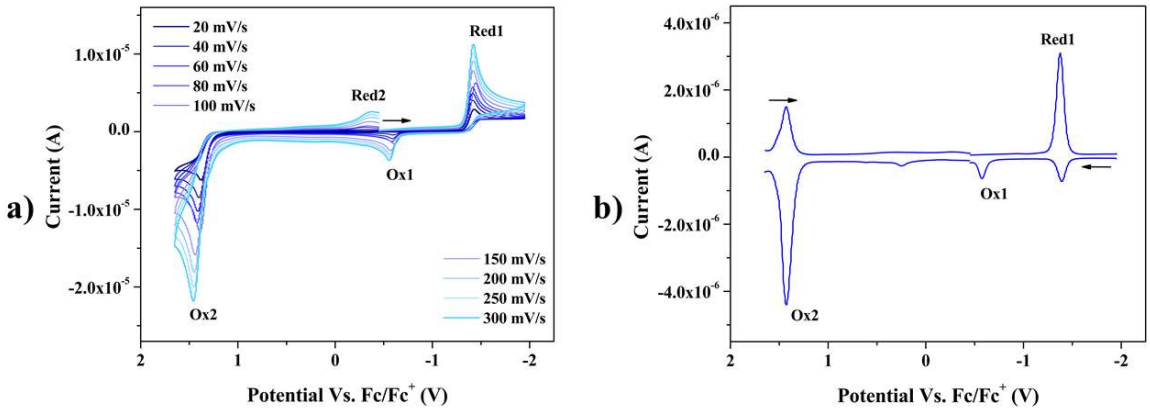

Fig. S38. CV recorded over 20-300 mV/s (a) and SQW voltammetry (b) for **P2**.

Table S1. Redox processes for DASAs and precursors observed in CV and SQW (process order is predicated on forward scan direction).

Compound	Ox1 $E_{1/2}$ V	Ox2 $E_{1/2}$ V	Red1 $E_{1/2}$ V	Red2 $E_{1/2}$ V	Red3 $E_{1/2}$ V
P1	-0.478	1.55	-1.42	-0.336	N/A
P2	-0.565	1.45	-1.44	-0.364	N/A
1	0.190	0.706	-0.313	-1.61	N/A
2	0.166	0.724	-0.363	-1.60	N/A
3	0.118	0.730	-0.418	-0.776	-1.58
4	0.111	0.539	-0.435	-1.59	N/A
5	0.0840	0.558	-0.519	-1.58	N/A
6	0.0355	0.823	-0.492	-0.933	-1.57

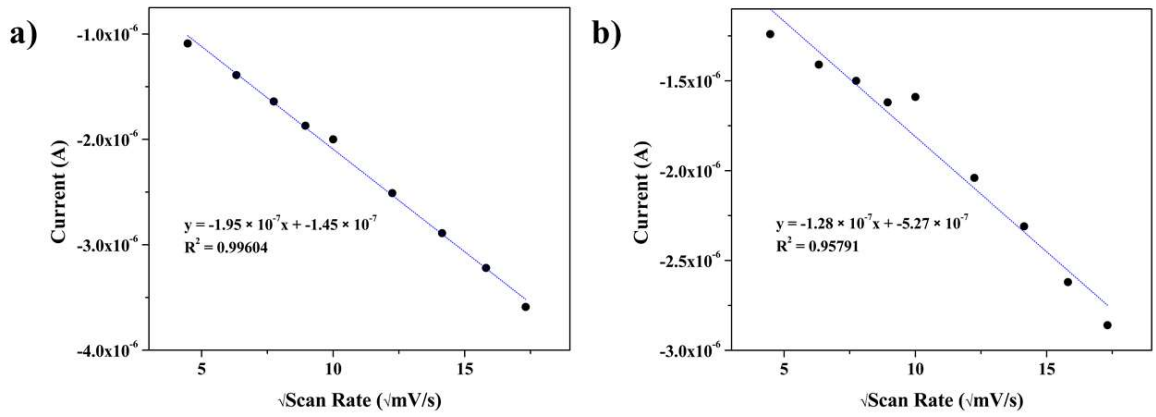

Fig. S39. Scan-rate dependence (20-300 mV/s) for 'Ox1' (a) and 'Ox2' (b) processes in **1** with linear regression provided.

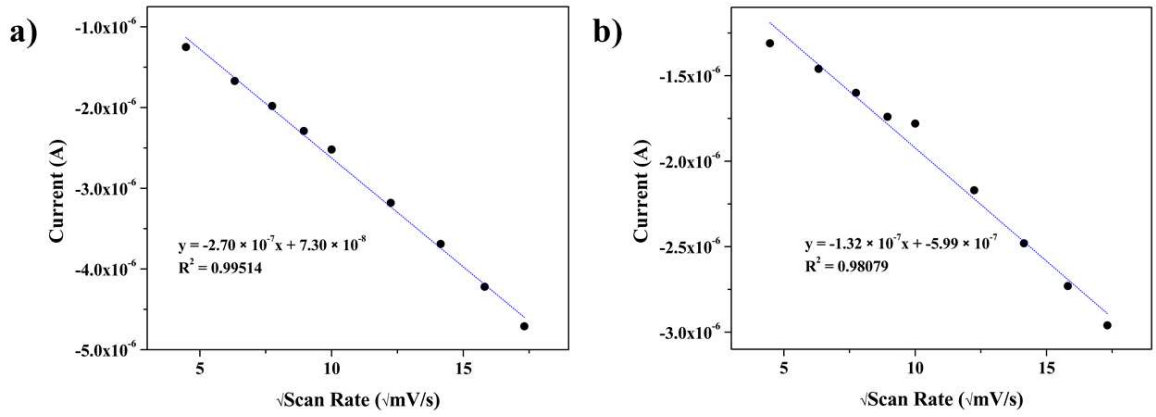

Fig. S40. Scan-rate dependence (20-300 mV/s) for 'Ox1' (a) and 'Ox2' (b) processes in **2** with linear regression provided.

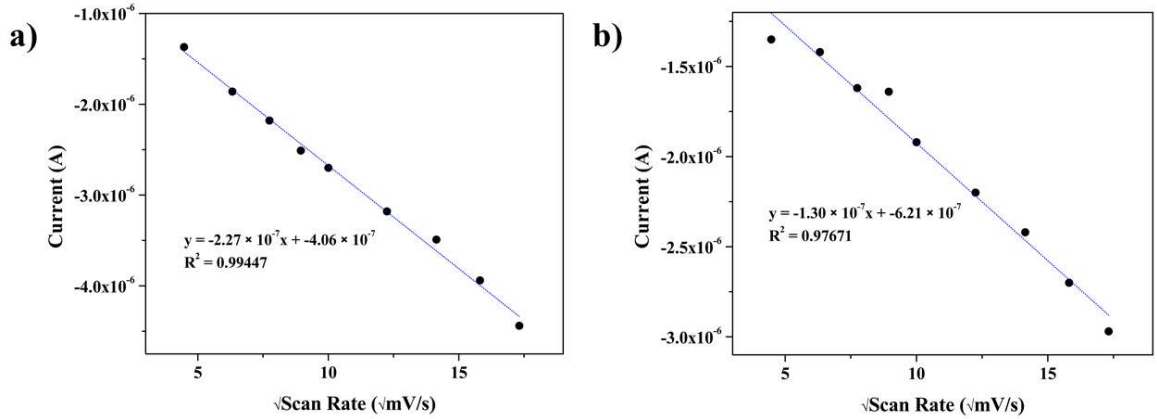

Fig. S41. Scan-rate dependence (20-300 mV/s) for 'Ox1' (a) and 'Ox2' (b) processes in **3** with linear regression provided.

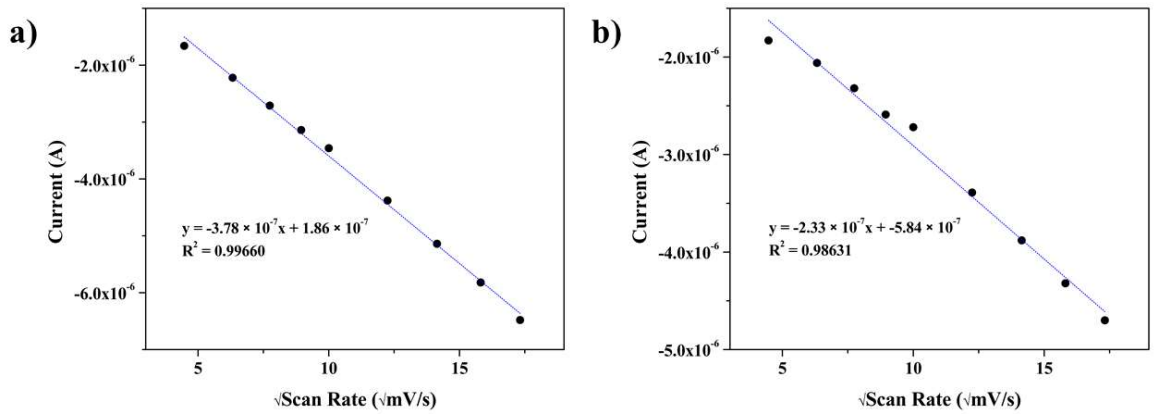

Fig. S42. Scan-rate dependence (20-300 mV/s) for 'Ox1' (a) and 'Ox2' (b) processes in **4** with linear regression provided.

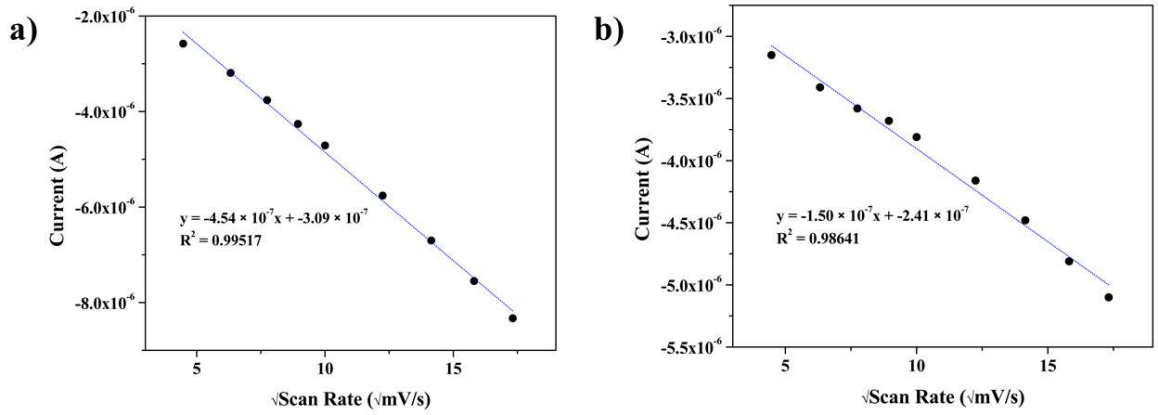

Fig. S43. Scan-rate dependence (20-300 mV/s) for 'Ox1' (a) and 'Ox2' (b) processes in **5** with linear regression provided.

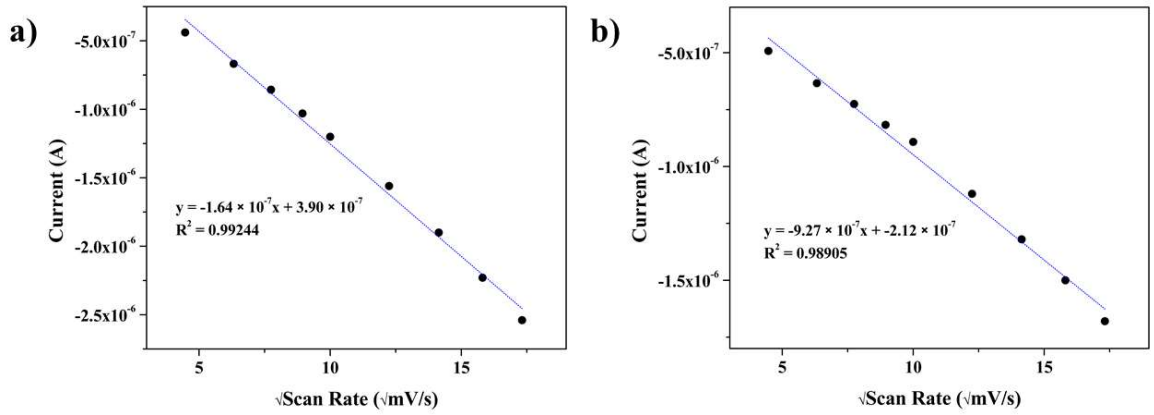

Fig. S44. Scan-rate dependence (20-300 mV/s) for 'Ox1' (a) and 'Ox2' (b) processes in **6** with linear regression provided.

In addition to the oxidation processes discussed, voltammograms for DASA compounds (Fig. 2a-b, ESI†, Fig. S31-S35, Table S1) exhibited a reduction that occurred at $E_{1/2} \approx -1.59$ V. The process was not

expected to be linked the photo-cyclisation associated with DASA photo-switching as it was also observed in both DASA precursors **P1** and **P2** (ESI†, Fig. S36 and S37, Table S1). The 'Red2' process at $E_{1/2} \approx -0.855$ V for **3** and **6** (ESI†, Fig. S32 and S35, Table S1) was only observed for these compounds, and was tentatively attributed to the cyclisation.

S7. Spectroelectrochemistry (SEC)

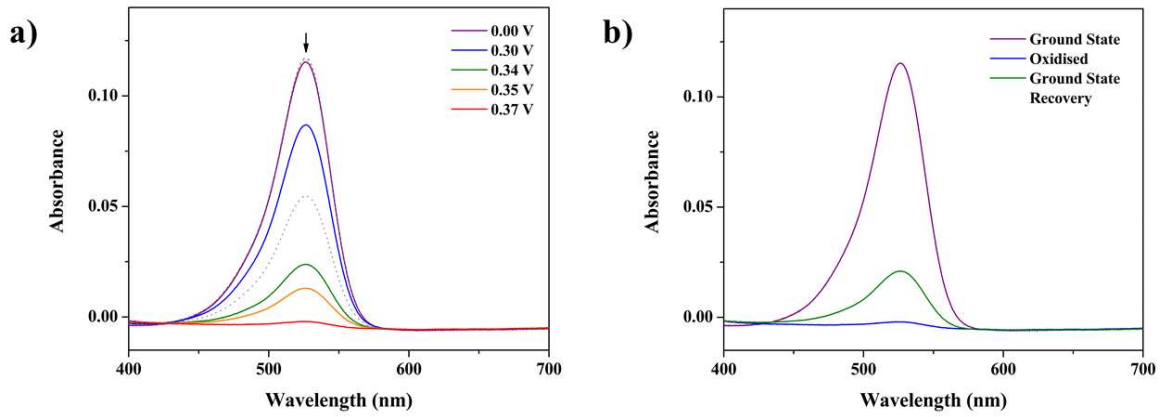

Fig. S45. UV-vis SEC spectra from 400-700 nm (a) and UV-vis spectra following SEC indicating thermodynamic recovery in the same range (b) for **2**.

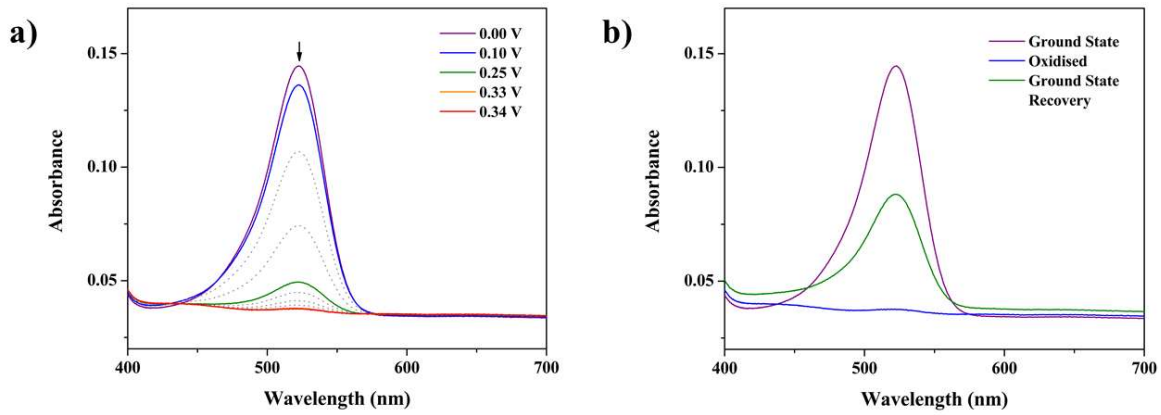

Fig. S46. UV-vis SEC spectra from 400-700 nm (a) and UV-vis spectra following SEC indicating thermodynamic recovery in the same range (b) for **3**.

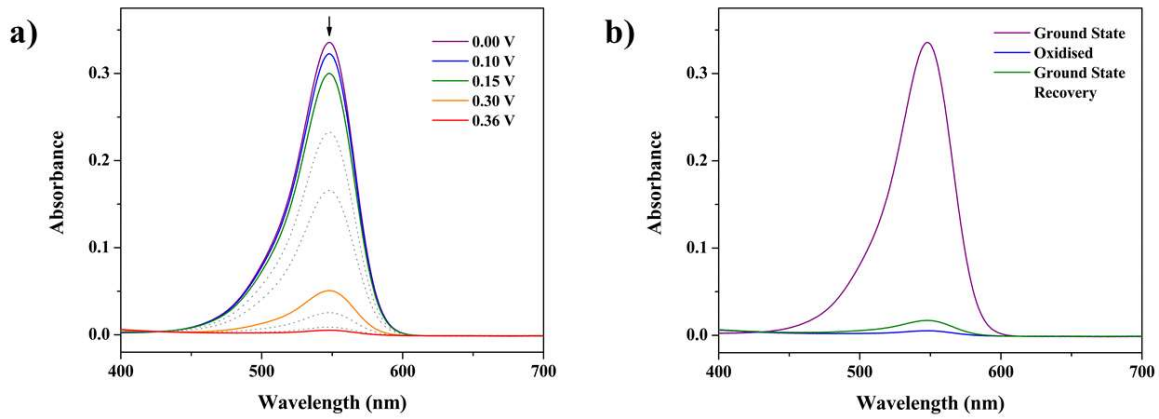

Fig. S47. UV-vis SEC spectra from 400-700 nm (a) and UV-vis spectra following SEC indicating thermodynamic recovery in the same range (b) for **4**.

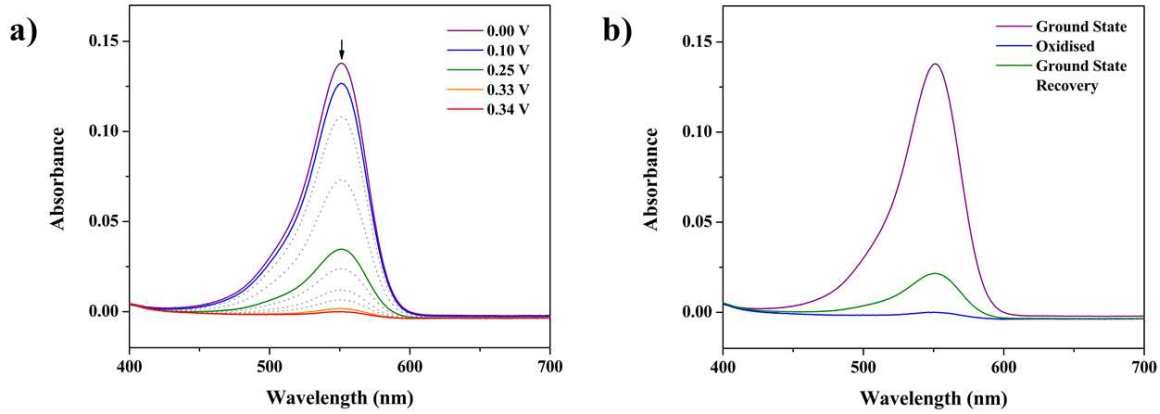

Fig. S48. UV-vis SEC spectra from 400-700 nm (a) and UV-vis spectra following SEC indicating thermodynamic recovery in the same range (b) for **5**.

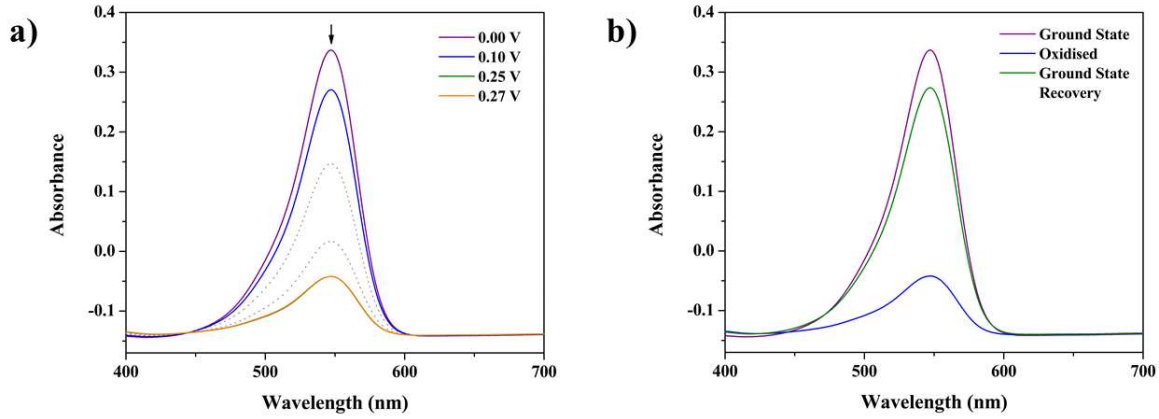

Fig. S49. UV-vis SEC spectra from 400-700 nm (a) and UV-vis spectra following SEC indicating thermodynamic recovery in the same range (b) for **6**.

Table S2. Redox processes for DASAs and precursors observed in CV and SQW (process order is predicated on forward scan direction).

Compound	Excitation Potential (V)	Thermodynamic Recovery (%)
1	0.44	13
2	0.37	20
3	0.34	47
4	0.36	4
5	0.34	16
6	0.25	83

References

[1] Fulmer, G. R.; Miller, A. J. M.; Sherden, N. H.; Gottlieb, H. E.; Nudelman, A.; Stoltz, B. M.; Bercaw, J. E.; Goldberg, K. I. NMR Chemical Shifts of Trace Impurities: Common Laboratory Solvents, Organics, and Gases in Deuterated Solvents Relevant to the Organometallic Chemist. *Organometallics* **2010**, *29* (9), 2176–2179. https://doi.org/10.1021/om100106e.

[2] Helmy, S.; Oh, S.; Leibfarth, F. A.; Hawker, C. J.; Read De Alaniz, J. Design and Synthesis of Donor-Acceptor Stenhouse Adducts: A Visible Light Photoswitch Derived from Furfural. *J. Org. Chem.* **2014**, *79* (23), 11316–11329. https://doi.org/10.1021/jo502206g.

[3] Helmy, S.; Leibfarth, F.; Oh, S.; Poelma, J.; Hawker, C. J.; Read De Alaniz, J. Photoswitching Using Visible Light: A New Class of Organic Photochromic Molecules. *J. Am. Chem. Soc.* **2014**, *136* (23), 8169–8172. https://doi.org/10.1021/ja503016b.

[4] Larkin, P. J. Illustrated IR and Raman Spectra Demonstrating Important Functional Groups. In *Infrared and Raman Spectroscopy*; 2018; pp 153–210. https://doi.org/10.1016/b978-0-12-804162-8.00008-2.